IOPscience iopscience.iop.org

Home Search Collections Journals About Contact us My IOPscience

Modelling of visible and near infrared wavelength quantum well devices made of zinc-blende $In_xGa_{1-x}N$

This article has been downloaded from IOPscience. Please scroll down to see the full text article.

2004 J. Phys.: Condens. Matter 16 511

(http://iopscience.iop.org/0953-8984/16/3/027)

View the table of contents for this issue, or go to the journal homepage for more

Download details:
IP Address: 129.252.86.83
The article was downloaded on 28/05/2010 at 07:53

Please note that terms and conditions apply.

INSTITUTE OF PHYSICS PUBLISHING JOURNAL OF PHYSICS: CONDENSED MATTER

J. Phys.: Condens. Matter **16** (2004) 511–519 PII: S0953-8984(04)65523-8

Modelling of visible and near infrared wavelength quantum well devices made of zinc-blende $In_xGa_{1-x}N$

A Bhouri[1], H Mejri[1], F Ben Zid[1], H Belmabrouk[1], M Said[1], N Bouarissa[2] and J-L Lazzari[3]

[1] Unité de Physique des Solides, Département de Physique, Faculté des Sciences, 5019 Monastir, Tunisia
[2] Physics Department, University of M'sila, 28000 M'sila, Algeria
[3] Centre de Recherche sur les Mécanismes de la Croissance Cristalline, CRMC2, UPR-CNRS 7251,[4] Campus de Luminy, Case 913, 13288 Marseille cedex 9, France

E-mail: bhouri_amel@yahoo.fr

Received 2 July 2003, in final form 30 October 2003
Published 9 January 2004
Online at stacks.iop.org/JPhysCM/16/511 (DOI: 10.1088/0953-8984/16/3/027)

Abstract

We report band offset calculations for lattice-matched and pseudomorphically strained $In_xGa_{1-x}N/In_yGa_{1-y}N$ heterointerfaces using the model solid theory combined with *ab initio* calculations. From the results obtained, we have calculated the bandgap of bulk $In_xGa_{1-x}N$ on GaN as a function of the indium composition. We have also simulated the band edges of an $In_xGa_{1-x}N$/GaN heterostructure. A self-consistent analysis is made to investigate the effect of strains on the interband transitions with the aim of achieving emissions at both visible and near infrared wavelengths. An attempt to explain the results obtained will be presented.

1. Introduction

In recent years, important developments have occurred in the epitaxy of small-structure systems and their applications in microelectronic and optoelectronic devices. With the advent of this class of materials, the effect of alloy composition, size quantization, device geometry, doping modulation and lattice strains can be combined to achieve extra flexibility for tailoring the electronic band structure. As regards the III–V compounds based on GaAs, most research activities were usually concentrated on the fabrication of devices designed to operate in the visible. At present, there is a large potential for the development of lasers and light emitting diodes (LEDs) working in the ultraviolet with use of $Al_xGa_{1-x}N$ [1]. Another ternary alloy, $In_xGa_{1-x}N$, has the advantage of growing coherently on GaN and it appears to be useful as quantum well (QW) layers in blue laser diodes [2]. The use of this material as a basic constituent in green LEDs and laser diodes is believed to be occurring [3].

[4] Laboratoire associé aux Universités Aix-Marseille II et III.

 © 2004 IOP Publishing Ltd Printed in the UK

From a fundamental viewpoint, to simulate heterostructures based on $In_xGa_{1-x}N$, it is required to know the bandgap energy, the electron and hole effective masses and the band offsets as well as their composition dependences. As regards the bandgap energy and the effective masses of unstrained $In_xGa_{1-x}N$, empirical pseudopotential calculations have been done by taking for the intrinsic InN bandgap the commonly accepted value of 1.94 eV [4]. However, recent advances in the epitaxial growth of single-crystal InN have led to a drastic re-evaluation of the fundamental energy gap for this compound. This gap has been unambiguously determined to be in the range 0.7–0.8 eV using optical absorption, photoluminescence and photomodulated reflectance experiments [5–7]. No systematic calculations of the bandgap energy and the band offsets have been carried out for this ternary under strain. The lack of information on these electronic band parameters has prompted us to perform such a calculation using the model solid theory [8] as we have previously done for $Si_{1-x}Ge_x$ [9] and $Al_{1-x}Ga_xN$ [10]. Moreover, an understanding of optical properties of $In_xGa_{1-x}N$ is essential for device design. Accurate knowledge about recombination mechanisms in $In_xGa_{1-x}N$-related heterostructures remains rather limited due partially to the absence of theoretical predictions. With this in mind, we have modelled $In_xGa_{1-x}N$/GaN heterostructures for different indium compositions and well layer thicknesses. The calculations are intended to optimize emissions in the visible and near infrared wavelength domains. To analyse the optical behaviour of the heterostructures under investigation, we have calculated the strain-dependent oscillator strengths for interband transitions in the channel QW.

The paper is organized as follows: after a brief introduction, we report in section 2 results on the band offsets at $In_xGa_{1-x}N/In_yGa_{1-y}N$ strained/relaxed interfaces calculated as a function of indium compositions x and y; in section 3, we present a modelling of an $In_xGa_{1-x}N$/GaN heterostructure; conclusions are summarized in section 4.

2. Calculated band offsets for (001)-oriented $In_xGa_{1-x}N/In_yGa_{1-y}N$ interfaces

Zinc-blende GaN and InN have lattice constants of 0.450 and 0.498 nm respectively [11]. Pseudomorphic growth along the $\langle 001\rangle$ direction of an $In_xGa_{1-x}N$ layer on an $In_yGa_{1-y}N$ substrate with a lattice mismatch subjects the overlayer to a biaxial strain in the (001) plane and to a uniaxial strain perpendicular to the interface. The effect of these strains on energy levels can be decomposed into hydrostatic and shear contributions. The hydrostatic strain shifts the average valence band energy as well as the conduction band, whereas the shear strain splits degenerate bands and leads to an additional splitting of the valence band when coupled to the spin–orbit interaction. For the $In_xGa_{1-x}N$ material under investigation, the conduction band is of Γ character over the whole range of composition x. As a consequence, the latter strain component has no effect on the energetic position of this band. For a (001) heterojunction in the $In_xGa_{1-x}N/In_yGa_{1-y}N$ system, the strain-dependent shifts of the valence bands relative to their unstrained positions are given by [8–10]

$$\begin{aligned}
\delta E_{\mathrm{v,av}}^{\mathrm{hy}} &= a_{\mathrm{v}}(2\varepsilon_{\parallel} + \varepsilon_{\perp}) - \tfrac{1}{2}\delta E_{001} \\
\delta E_{\mathrm{lh}}^{\mathrm{sh}} &= a_{\mathrm{v}}(2\varepsilon_{\parallel} + \varepsilon_{\perp}) - \tfrac{1}{2}\Delta_0 + \tfrac{1}{4}\delta E_{001} + \tfrac{1}{2}[\Delta_0^2 + \Delta_0\delta E_{001} + \tfrac{9}{4}(\delta E_{001})^2]^{1/2} \\
\delta E_{\mathrm{so}}^{\mathrm{sh}} &= a_{\mathrm{v}}(2\varepsilon_{\parallel} + \varepsilon_{\perp}) + \tfrac{1}{2}\Delta_0 + \tfrac{1}{4}\delta E_{001} - \tfrac{1}{2}[\Delta_0^2 + \Delta_0\delta E_{001} + \tfrac{9}{4}(\delta E_{001})^2]^{1/2}
\end{aligned} \tag{1}$$

and similarly for the conduction band:

$$\delta E_{\mathrm{c}}^{\mathrm{hy}} = a_{\mathrm{c}}(2\varepsilon_{\parallel} + \varepsilon_{\perp}) \tag{2}$$

with

$$\varepsilon_{\parallel} = \frac{a_{\parallel}}{a} - 1, \qquad \varepsilon_{\perp} = \frac{a_{\perp}}{a} - 1,$$

$$a_{\parallel} = a_0,$$
$$a_{\perp} = a\left[1 - 2\frac{C_{12}}{C_{11}}\left(\frac{a_0}{a} - 1\right)\right]$$

and

$$\delta E_{001} = 2b(\varepsilon_{\perp} - \varepsilon_{\parallel})$$

where a_v and a_c represent the hydrostatic deformation potentials for the valence and conduction bands, $\varepsilon_{\parallel}$ and $\varepsilon_{\perp}$ are the in-plane and the perpendicular-to-the-interface strains, a_0 and a are the substrate and the overlayer lattice constants, C_{11} and C_{12} are the elastic constants of the epitaxial layer material, Δ_0 is the spin–orbit splitting and b denotes the shear deformation potential for the valence band. The subscripts hh, lh and so refer to heavy hole, light hole and spin–orbit split-off bands. According to equations (1) and (2), the band offsets at the $In_xGa_{1-x}N/In_yGa_{1-y}N$ heterointerfaces can be derived by simply subtracting the values of E_v and E_c of individual semiconductors. Their expressions are as follows:

$$\Delta E_{v_{hh,lh}} = \Delta E_v^{uns} + \delta E_{v_{hh,lh}} \tag{3}$$

and

$$\Delta E_c = \Delta E_v^{uns} + \Delta E_g^{uns} + \delta E_c \tag{4}$$

where ΔE_v^{uns} is the natural valence band discontinuity, ΔE_g^{uns} represents the bandgap difference between the unstrained materials constituting the heterojunction and $\delta E_{v_{hh,lh}}$ and δE_c are the strain-dependent shifts of the valence and conduction bands defined above. Table 1 presents the values of E_v^{uns} as calculated by Wei and Zunger [12] for GaN and InN and those of a, C_{11}, C_{12}, Δ_0, a_c, a_v and b [11, 13–17]. For the $In_xGa_{1-x}N$ ternary alloy, a linear interpolation seems to be a good approximation for evaluating these parameters. The data obtained enabled us to calculate, using equations (1)–(4), the band offsets for lattice-matched and pseudomorphically strained $In_xGa_{1-x}N/In_yGa_{1-y}N$ as a function of compositions x and y. The results are depicted in figure 1. As seen, plot 1(b) distinguishes between hh (solid lines) and lh (dotted lines) band offsets. The separation in the valence band offsets is of interest in separately evaluating the confinements of the two types of holes in $In_xGa_{1-x}N$ QW structures. The law $\Delta E_{v,hh} \cong (x - y)(0.77 - 0.21x + 0.95 \times 10^{-2}\, x^2)$ gives an approximate analytical expression for the heavy hole valence band discontinuity. The errors on the three constants of this fit are mainly less than 1%. However, for light holes and conduction electrons, the band offsets cannot be fitted similarly by simple polynomial functions. As can be noted from the band offset plots 1(a) and (b):

(i) the line-up at $In_xGa_{1-x}N/In_yGa_{1-y}N$ strained/relaxed heterointerfaces is of 'type I' for $x > y$. This implies that the bandgap of the $In_xGa_{1-x}N$ overlayer falls completely into the gap of the $In_yGa_{1-y}N$ substrate.
(ii) In the case of $In_xGa_{1-x}N/In_yGa_{1-y}N$ with $x < y$, the band alignment is, on the contrary, of 'type I' in the relaxed $In_yGa_{1-y}N$ layer.

Let us now calculate the bandgap of bulk $In_xGa_{1-x}N$ on GaN substrate as a function of indium composition. Energies can be deduced from band offset calculations using the relationship

$$E_g^{str}(In_xGa_{1-x}N) = E_g(GaN) + \Delta E_c - \Delta E_{v,hh}. \tag{5}$$

The results are depicted in figure 2. In the plot, also reported is the bandgap versus x of unstrained $In_xGa_{1-x}N$ as calculated in the present work according to [5–7, 14, 18]. As seen, the bandgap of strained $In_xGa_{1-x}N$ shows a red-shift in energy with respect to its energetic position at zero strain, especially at high indium compositions. In addition, the x-dependence

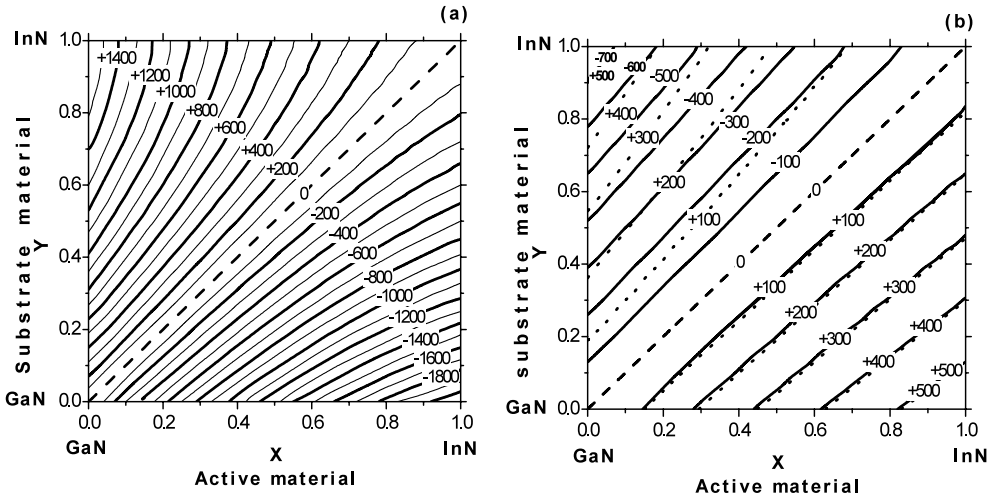

Figure 1. (a) Conduction band offsets $\Delta E_c = E_c(x) - E_c(y)$ and (b) valence band offsets $\Delta E_v = E_v(x) - E_v(y)$ for the heavy holes (solid lines) and light holes (dotted lines) at (001)-oriented $In_xGa_{1-x}N/In_yGa_{1-y}N$ heterointerfaces. The band offsets are in millielectronvolts.

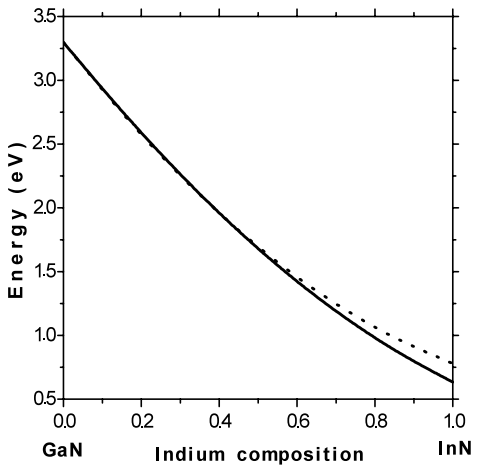

Figure 2. The x-dependent bandgap of strained (solid curve) and unstrained (dotted curve) $In_xGa_{1-x}N$.

of the strained bandgap can be fitted by the law $E_g^{str}(In_xGa_{1-x}N) = 3.302 - 3.829x + 1.157x^2$ with errors on the constants of the order of 5×10^{-4} eV. Like the bandgap, the bowing parameter of $In_xGa_{1-x}N$ decreases from 1.40 to 1.157 eV when it is subjected to strains.

In the following, we compare calculated band offsets with existing experimental and theoretical data for specific compositions in $In_xGa_{1-x}N/In_yGa_{1-y}N$ QW heterostructures. Van de Walle and Neugebauer [19] have calculated a valence band offset (VBO) of 0.3 eV for an unstrained GaN/InN interface in a cubic system. Wei *et al* [20] have obtained a value of 0.26 eV for the same heterointerface. The latter authors found a VBO of 0.48 eV for wurtzite GaN/InN. Experimentally, strain-induced piezoelectric fields significantly complicate any direct measurement of the GaN/InN band offset. According to [2], only one experimental

Table 1. Parameters used for the band offset calculations. All symbols have the meanings given in the text. In the table, are also reported values of the electron and hole effective masses in m_0 for GaN and InN.

	a (Å)	C_{11} (GPa)	C_{12} (GPa)	Δ_0 (eV)	E_v^{uns} (eV)	a_v (eV)	b (eV)	a_c (eV)	m_{hh}	m_{lh}	m_e
InN	4.98[a]	187[b]	125[b]	0.005[c]	−0.46[e]	−0.7[c]	−1.2[c]	−2.65[c]	0.84[d]	0.16[d]	0.07[e]
GaN	4.5[a]	293[b]	159[b]	0.017[c]	−0.72[e]	−0.69[c]	−2[c]	−6.71[c]	0.8[d]	0.18[d]	0.15[f]

[a] See [11].
[b] See [13].
[c] See [14].
[d] See [15].
[e] See [16].
[f] See [17].

study of the GaN/InN interface has been reported [21]. The value of 1.05 eV has been adopted for GaN/InN in the wurtzite phase. For zinc-blende GaN/InN, Vurgaftman *et al* [2] have recommended the value of 0.26 eV, obtained by Wei *et al* [20]. With the updated value of the bandgap in InN, the latter authors recommended a VBO of 0.3 eV for the zinc-blende InN/GaN interface and 0.5 eV for the wurtzite interface [14]. In the present work, we have obtained for the VBO in cubic GaN/InN and InN/GaN the values 0.77 and 0.57 eV respectively, meaning that the two are inequivalent and must be specified separately. Unlike the valence band case, there is no report of conduction band discontinuity for $In_xGa_{1-x}N$. Due to the lack in the band offset data, our systematic calculations, that have the advantage of including strain effects, can provide valuable information on the band discontinuities for $In_xGa_{1-x}N/In_yGa_{1-y}N$ strained/relaxed heterostructures in the zinc-blende phase.

3. Theoretical analysis of interband transitions in $In_xGa_{1-x}N$/GaN heterostructures

The confined heterostructure for modelling consists of an undoped $In_xGa_{1-x}N$ QW of thickness L, embedded between relatively thick GaN barriers. The thickness L and the indium composition x are treated as parameters. As demonstrated above, the band alignment for $In_xGa_{1-x}N$/GaN is of type I. This means that both electrons and holes are confined in the $In_xGa_{1-x}N$ well layer. The ground state of such a two-dimensional (2D) system can be simply described using the effective mass theory and the local density-functional formalism [22]. In the following, we consider the heterostructure at a constant temperature and no electric field is applied. In the one-band version of the envelope wavefunction approximation, the subband energies for the conduction and valence bands can be computed from the effective Hamiltonian:

$$H_{\text{eff}}(z) = -\frac{\hbar^2}{2}\frac{\mathrm{d}}{\mathrm{d}z}\frac{1}{m^*(z)}\frac{\mathrm{d}}{\mathrm{d}z} + V(z) \tag{6}$$

where z is the growth direction, $m^*(z)$ is the effective mass of free carriers, $V(z)$ is the total potential energy. Values of the electron and hole effective masses, as calculated for GaN and InN [16, 17], are listed in table 1. A linear interpolation is used to calculate these electronic band parameters for the $In_xGa_{1-x}N$ layers with different indium compositions. In evaluating the energy potential $V(z)$, the band offsets at the strained-layer interfaces were deduced from results of section 2. Using equation (6), we have calculated the conduction and valence band edges as well as the energy levels for the $In_xGa_{1-x}N$/GaN heterostructure. Figure 3 shows the electron and hole confinement energies versus the QW width for several indium compositions. As can be seen, the confinement energy decays as L increases and shows an

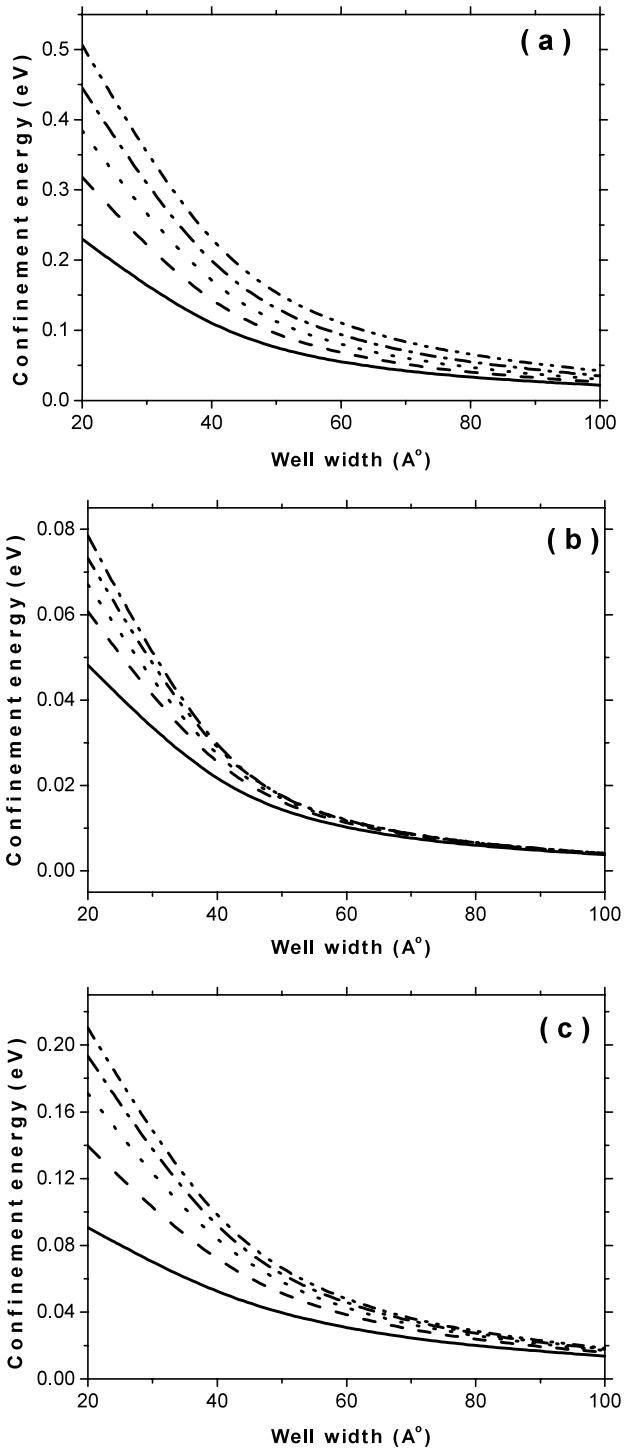

Figure 3. The confinement energy of conduction electrons (a), heavy holes (b) and light holes (c) as a function of well width for several indium compositions in the range $0.2 \leqslant x \leqslant 1.0$ (from the bottom to the top).

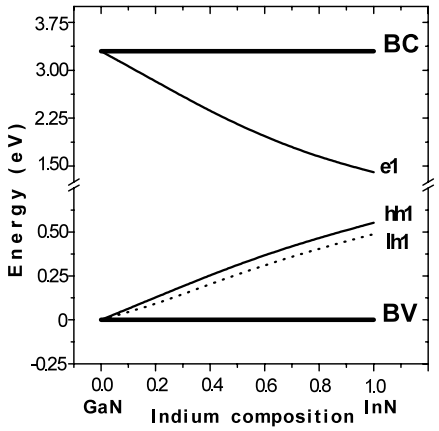

Figure 4. The subbands e1, hh1 and lh1 versus x for an $In_xGa_{1-x}N$/GaN heterostructure with a well 4 nm thick. Symbols CB and VB refer to the GaN band edges. The e1 $\rightarrow$ hh1 and e1 $\rightarrow$ lh1 energy emissions are shown as a separation between the subbands.

increasing tendency with x. As also shown, larger confinement can be achieved in narrow QWs and for relatively high indium molar fractions. The x-related shift of the subbands is due substantially to strain effects. In a QW device based on $In_xGa_{1-x}N$, this shift gives rise to an increase in the confinement and can simultaneously provide tunable wavelength transitions. To investigate the latter property, we have calculated the energies of both e1 $\rightarrow$ hh1 and e1 $\rightarrow$ lh1 transitions versus x and L. The subscripts e, hh, and lh refer to electrons, heavy holes and light holes. We report in figure 4 the x-dependent bandgap diagram of an $In_xGa_{1-x}N$/GaN heterostructure, as calculated for $L = 4$ nm. The plot shows GaN band edges and $In_xGa_{1-x}N$ subband energies with the emission energy as the separation between the subbands. It is clearly seen that the transitions e1 $\rightarrow$ hh1 and e1 $\rightarrow$ lh1 shift down in energy emission as the indium composition increases. They also show a red-shift with increasing L. Furthermore, the energy emission of these interband transitions in 4 nm thick QW ranges from 0.851 (1456.5) to 3.299 eV (375.7 nm). This means that the $In_xGa_{1-x}N$/GaN QW heterostructure can be seen to emit at both visible and near infrared wavelengths by simply monitoring the strain and the well layer thickness.

Another characteristic of an electron transition is the oscillator strength. It is defined, from an initial state $|\phi_1\rangle$ to a final state $|\phi_k\rangle$, by the relationship [23, 24]

$$f_{1\rightarrow k} = \frac{2m_0}{\hbar^2}(E_1 - E_k)|\langle\phi_1|z|\phi_k\rangle|^2, \tag{7}$$

where m_0 is the free electron mass, $\hbar$ is the Planck's constant, $(E_1 - E_k)$ is the energy difference between the initial and finite states and $|\langle\phi_1|z|\phi_k\rangle|$ is the dipole matrix element of the transition. We have calculated the strain-dependent oscillator strength for the interband transitions e1 $\rightarrow$ hh1 and e1 $\rightarrow$ lh1 using equation (7). Typical results, obtained for $L = 4$ nm, are shown in figure 5. As can be seen, the oscillator strengths $f_{e1\rightarrow lh1}$ and $f_{e1\rightarrow hh1}$ decrease as x increases going from GaN to InN. The same trend is observed for the x-dependent oscillator strengths when varying the well width. It is also shown from our calculations that this decrease does not significantly affect the interband transition oscillator strengths, which remain relatively high. This means that the efficiency of radiative recombination in $In_xGa_{1-x}N$ heterostructures is highly preserved. With a view to possible device application, attention is devoted to the blue, green and red emissions in $In_xGa_{1-x}N$/GaN heterostructures. From the calculated emission

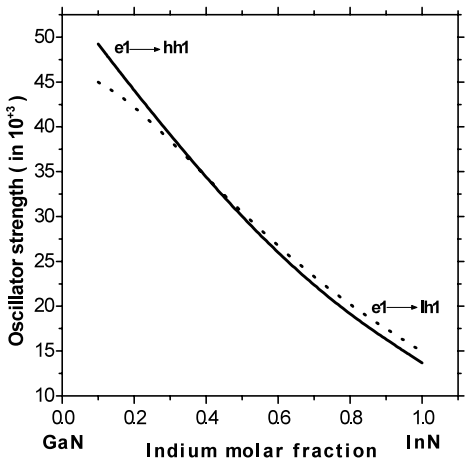

Figure 5. The oscillator strengths versus x for interband transitions e1 $\rightarrow$ hh1 (solid curve) and e1 $\rightarrow$ lh1 (dotted curve) relative to an $In_xGa_{1-x}N$ layer 4 nm thick.

Table 2. Values of indium compositions and oscillator strengths for blue (2.804 eV), green (2.409 eV) and red (1.925 eV) emissions in an $In_xGa_{1-x}N$/GaN heterostructure with $L = 2$, 4, 6, 8 and 10 nm (from the top to the bottom).

Indium composition			Oscillator strength (10^{+3})		
Blue	Green	Red	Blue	Green	Red
0.222	0.372	0.577	45.489	38.991	30.959
0.168	0.294	0.467	45.699	39.263	31.212
0.153	0.276	0.440	45.798	39.260	31.323
0.147	0.267	0.428	45.825	39.345	31.429
0.144	0.263	0.423	45.833	39.362	31.438

energy for the transition e1 $\rightarrow$ hh1, we deduce the indium compositions and the well layer thicknesses, which give rise to these lines at 2.804, 2.409 and 1.925 eV respectively. The relevant values are listed in table 2. In the table, also reported are the oscillator strengths for the three emissions. As shown, the indium molar fractions providing the blue line, for $2 \leqslant L \leqslant 10$ nm, range from 0.144 to 0.222, whereas emissions at the green and the red wavelengths are expected to occur for $0.263 \leqslant x \leqslant 0.372$ and $0.423 \leqslant x \leqslant 0.577$ respectively. Note that O'Donnell *et al* [3] have found for $In_xGa_{1-x}N$-related heterostructures that blue and green emissions occur in the indium composition range 0.2–0.45, result in agreement with our theoretical predictions.

4. Conclusion

Estimates of valence and conduction band offsets for $In_xGa_{1-x}N/In_yGa_{1-y}N$ strained/relaxed heterointerfaces are presented. The bandgap of bulk $In_xGa_{1-x}N$ has also been calculated as a function of composition x. From the electronic band parameters obtained, we simulated the band edges of an $In_xGa_{1-x}N$/GaN heterostructure. A theoretical analysis of the strain-dependent interband transitions has been made in order to investigate the optical properties of this heterostructure. A peculiar feature was revealed: the $In_xGa_{1-x}N$ channel can emit photon energies in the spectral range 0.680–3.299 eV with relatively high oscillator strengths. From

a fundamental viewpoint, the study of strain-dependent transitions gives useful information on the free carrier distribution, the potential profile and the coupling between electron and hole gases within the heterostructure. This investigation is of great interest in technological applications as well, especially for designing devices made of $In_xGa_{1-x}N$ intended to operate at the visible and near infrared wavelengths.

Acknowledgments

One of us (NB) would like to thank the Faculty of Science, Monastir, Tunisia, in particular the UR of Solid State Physics, for their financial support and kind hospitality during his stay at Monastir. Part of this work was done at the International Centre for Theoretical Physics (ICTP) Trieste, Italy. NB and MS gratefully acknowledge the ICTP support during their stay at the Centre.

References

[1] Angerer H, Brunner D, Freudenberg F, Ambacher O, Stutzmann M, Höpler R, Metzger T, Born E, Dollinger G, Bergmaier A, Karsch S and Körner H-J 1997 *Appl. Phys. Lett.* **71** 1504
[2] Vurgaftman I, Meyer J R and Ram-Mohan L R 2001 *J. Appl. Phys.* **89** 5815 and references therein
[3] O'Donnell K P, Martin R W and Middleton P G 1999 *Phys. Rev. Lett.* **82** 237
[4] Kassali K and Bouarissa N 2000 *Solid-State Electron.* **44** 501
[5] Wu J, Walukiewicz W, Yu K M, Ager J W III, Haller E E, Lu H, Schaff W J, Saito Y and Nanishi Y 2002 *Appl. Phys. Lett.* **80** 3967
[6] Masuoka T, Okamoto H, Nakao M, Harima H and Kurimoto E 2002 *Appl. Phys. Lett.* **81** 1246
[7] Davydov V Yu *et al* 2002 *Phys. Status Solidi* b **229** R1
[8] Van de Walle C G and Martin R 1986 *Phys. Rev.* B **34** 5621
Van de Walle C G 1989 *Phys. Rev.* B **39** 1871
[9] Ben Zid F, Bhouri A, Mejri H, Tlili R, Said M, Lazzari J-L, d'Avitaya F and Derrien J 2002 *J. Appl. Phys.* **91** 9170
[10] Bhouri A, Ben Zid F, Mejri H, Ben Fredj A, Bouarissa N and Said M 2002 *J. Phys.: Condens. Matter* **14** 7017
[11] Stampfl C and Van de Walle C G 1999 *Phys. Rev.* B **59** 5521
[12] Wei S-H and Zunger A 1998 *Appl. Phys. Lett.* **72** 2011
[13] Wright A F 1997 *J. Appl. Phys.* **82** 2833
[14] Vurgaftman I and Meyer J R 2003 *J. Appl. Phys.* **94** 3675 and references therein
[15] Pugh S K, Dugdale D J, Brand S and Abram R A 1999 *Semicond. Sci. Technol.* **14** 23
[16] Wu J, Walukiewicz W, Shan W, Yu K M, Ager J W III, Haller E E, Lu H and Schaff W J 2002 *Phys. Rev.* B **66** 201403
[17] Fancuilli M, Lei T and Moustakas T D 1993 *Physica* B **48** 15144
[18] Wu J, Walukiewicz W, Yu K M, Ager J W III, Haller E E, Lu H and Schaff W J 2002 *Appl. Phys. Lett.* **80** 4741
[19] Van de Walle C G and Neugebauer J 1997 *Appl. Phys. Lett.* **70** 2577
[20] Wei S-H and Zunger A 1996 *Appl. Phys. Lett.* **69** 2719
[21] Martin G A, Botchkarev A, Rockett A and Morkok H 1996 *Appl. Phys. Lett.* **68** 2541
[22] Hohenberg P and Kohn W 1964 *Phys. Rev.* B **136** 864
[23] Chen W Q and Andersson T G 1993 *J. Appl. Phys.* **73** 4484
[24] Mejri H, Ben Zid F, Bhouri A, Ben Fredj A, Said M, Lazzari J L and Derrien J 2002 *Physica* B **332** 37